Distortion-dependent Raman spectra and mode mixing in $R\mathrm{MnO_3}$ perovskites (R=La,Pr,Nd,Sm,Eu,Gd,Tb,Dy,Ho,Y)

M. N. Iliev,[1] M. V. Abrashev,[2] J. Laverdière,[3] S. Jandl,[3] M. M. Gospodinov,[4] Y.-Q. Wang,[1] and Y.-Y. Sun[1]
[1]*Texas Center for Superconductivity and Department of Physics, University of Houston, Houston, Texas 77204-5002, USA*
[2]*Faculty of Physics, University of Sofia, 1164 Sofia, Bulgaria*
[3]*Département de Physique, Université de Sherbrooke, Sherbrooke, Canada J1K 2R1*
[4]*Institute of Solid State Physics, Bulgarian Academy of Sciences, 1184 Sofia, Bulgaria*
(Received 19 September 2005; revised manuscript received 7 November 2005; published 16 February 2006)

The polarized Raman spectra of orthorhombic $R\mathrm{MnO_3}$ series (R=La,Pr,Nd,Sm,Eu,Gd,Tb,Dy,Ho,Y) were studied at room temperature. The variation of phonon frequencies with R ionic radius r_R as a whole confirms the commonly accepted Raman line assignments with two noticeable exceptions: (1) with decreasing r_R the stretching $A_g(1)$ and bending $A_g(3)$ modes strongly mix for R=Sm to Tb, while for further decrease or r_R (R=Dy,Ho,Y) the $A_g(3)$ mode is observed at higher frequency than $A_g(1)$ mode; (2) similar distortion-dependent mode mixing takes place for the rotational $A_g(2)$ and O1(x) [$A_g(7)$] modes. The mode mixing is particularly strong for the $R\mathrm{MnO_3}$ compounds with r_R values close to the transition from A type to incommensurate sinusoidal antiferromagnetic ordering at low temperatures. The frequency of rotational $A_g(2)$ and $A_g(4)$ modes scales to the angles of $\mathrm{MnO_6}$ [101] and [010] rotations, respectively, and could be used as a measure of their value.

DOI: 10.1103/PhysRevB.73.064302 PACS number(s): 78.30.−j, 63.20.Dj, 75.47.Lx

I. INTRODUCTION

Until recently the $R\mathrm{MnO_3}$ perovskites (R=rare earth, Y,Sc) have been the object of research mainly as parent materials of mixed valence manganites exhibiting colossal magnetoresistivity (CMR).[1–4] In the past few years, however, there is an increased interest in the complex relationships among the lattice distortions, magnetism, dielectric, and transport properties of undoped $R\mathrm{MnO_3}$.[5–10] In particular, it has been found that with the decreasing radius (r_R) of R (R=La to Eu) the transition temperature T_N to the A-type antiferromagnetic (A-AFM) structure also decreases. With the further decrease of r_R (R=Gd to Ho) the magnetic structure below T_N changes from A-AFM to an incommensurate antiferromagnetic one (IC-AFM) with sine-wave ordering of the Mn moments with temperature-dependent wave vector $\vec{k}_s=(k_s,0,0)$ along the a axis (in $Pnma$ notations). At $T_{lock}<T_N$, k_s locks at a value <0.4.[8] A transition to the commensurate E-type antiferromagnetic structure (E-AFM, $k_s=0.5$) has been observed below $T_{lock}=26$ K only for $\mathrm{HoMnO_3}$.[6] For $T<T_{lock}$, $\mathrm{TbMnO_3}$ and $\mathrm{DyMnO_3}$ exhibit ferroelectric order associated with lattice modulation.[7,9] Large magnetodielectric effects have also been reported for orthorhombic $\mathrm{HoMnO_3}$, and $\mathrm{YMnO_3}$.[11]

Although the role of lattice distortions in the interplay of magnetic, dielectric, and transport properties of $R\mathrm{MnO_3}$ perovskites is widely recognized, there are relatively few studies on the variations of these distortions with R.[10,12] Raman spectroscopy can provide significant additional information on the distortions and their variations with both R and temperature. The Raman active modes in $R\mathrm{MnO_3}$ ($7A_g+5B_{1g}+7B_{2g}+5B_{3g}$) are activated exclusively due to the deviations from ideal perovskite structure and in principle the activation of each Raman line can with definite certainty be assigned to the value of one or two types of basic distortion (rotations of $\mathrm{MnO_6}$ octahedra around [101] or [010] directions, Jahn-Teller distortion, or shift of R atoms).[13] The assignment of the Raman lines in the spectra of $R\mathrm{MnO_3}$ to definite atomic vibrations has been done by comparison of experimentally obtained Raman phonon frequencies of $\mathrm{LaMnO_3}$ and $\mathrm{YMnO_3}$ with those predicted by lattice dynamical calculations (LDC).[14] Although for most of the experimentally observed Raman lines the frequencies have been in good agreement with those predicted by LDC, some uncertainties about the phonon line assignment remained. Indeed, some Raman lines of the same symmetry have close frequencies and due to the approximations of the LDC model one reasonably expects some difference between measured and calculated values. The assignment of the two A_g Raman lines between 450 and 520 $\mathrm{cm^{-1}}$, where the A_g modes are corresponding to antistretching (AS) and bendings (B) of $\mathrm{MnO_6}$ octahedra, has been challenged by Martin-Carron *et al.*[15] in a Raman study of several $R\mathrm{MnO_3}$ perovskites (R=La,Pr,Nd,Tb,Ho,Er,Y). Based on the fact that the Mn-O distances exhibit only small changes within the $R\mathrm{MnO_3}$ series, they assigned the AS band observed near 480–490 $\mathrm{cm^{-1}}$ to the antistretching mode, while the B band which shifts from $\approx$450 $\mathrm{cm^{-1}}$ in $\mathrm{LaMnO_3}$ to $\approx$530 $\mathrm{cm^{-1}}$ in $\mathrm{ErMnO_3}$ has been assigned to bending mode(s). An obvious problem of this reassignment is the "crossing" of the AS and B modes, which are of the same A_g symmetry.

In this paper we present results of a detailed study of polarized Raman spectra of $R\mathrm{MnO_3}$ (R=La,Pr,Nd,Sm,Eu,Gd,Tb,Dy,Ho,Y) at room temperature. The comparison of variations with R of phonon frequencies and relative intensities of most pronounced A_g and B_{2g} modes shows that some corrections of the previous phonon mode assignment are needed. The strong mixing and spectral weight transfer between A_g antistretching (AS) and bending (B) modes in the 500 $\mathrm{cm^{-1}}$ region, most clearly observed for R=Eu,Gd,

and Tb, correlates with changes of magnetic structure. Similar distortion-dependent mode mixing is observed for the rotational $A_g(2)$ and O1(x) [$A_g(7)$] modes.

II. SAMPLES AND EXPERIMENTAL

$PrMnO_3$, $NdMnO_3$, and $SmMnO_3$ samples were grown by the floating zone method described in Ref. 16. Single crystals of $DyMnO_3$ of average sizes $1\times1\times2$ mm^3 were prepared following a procedure to be described elsewhere.[17] Orthorhombic $YMnO_3$, $HoMnO_3$ samples were prepared under pressure as described in Ref. 11. For R=Eu,Gd,Tb the precursor powders were heated at 1130–1160 °C in O_2 for 24 h. Although the samples (except for $DyMnO_3$) were polycrystalline, the size of the constituting microcrystals was larger than the laser spot. It was possible to select microcrystals with crystallographic orientation such that the spectra in parallel and crossed scattering configurations were dominated by A_g or B_{2g} contributions, respectively. For the exact separation of the A_g and B_{2g} spectra the SPECTRA SUBTRACT program of the GRAMS AI software package was used.

The Raman spectra were measured at room temperature in backscattering configuration using two different spectrometers: Labram-800 and Jobin Yvon HR640, both equipped with a microscope and liquid-nitrogen cooled charge-coupled device (CCD) detector. The spectra obtained with 514.5 nm (Ar^+) and 632.8 nm (He-Ne) were practically identical.

III. RESULTS AND DISCUSSION

The A_g and B_{2g} spectra of RMnO$_3$ as obtained at room temperature are shown in Fig. 1. With same scattering configuration, the absolute value of Raman intensities were increasing with decreasing R ionic radius (r_R). For better comparison the A_g and B_{2g} spectra were normalized to the integrated intensities of $A_g(1)+A_g(3)$ and $B_{2g}(1)$ lines, respectively. At least five A_g and four B_{2g} lines are clearly pronounced and the variations of their frequencies with R can be followed with a good accuracy. The variations with R of the line widths are likely related to the different sample growth technologies used. The weak broad band near 650 cm^{-1} in the A_g spectra is not a proper Raman mode.[14,18] The phonon line frequencies are given in Table I.

The correlation between structural and physical parameters of RMnO$_3$ perovskites may be described as a function of different parameters, such as the ionic radius r_R, tolerance factor t or the averaged tilt angle Ψ. The relation between these parameters, however, is close to linear[10] and any one of them can be used for characterization of phonon mode frequency variations. Figure 2 shows the dependence of Raman phonon frequencies on r_R. Most Raman frequencies ω_i exhibit nearly linear increase with r_R, but the slope $\Delta\omega_i/\Delta r_R$ depends mainly on the type of the mode (stretching, bending, or rotational) as well on the type of distortion that has activated the corresponding mode in the Raman spectrum (MnO_6 rotations around $[010]_c$ or $[101]_c$ cubic axes, Jahn-Teller (JT) distortion, and R shift).[13]

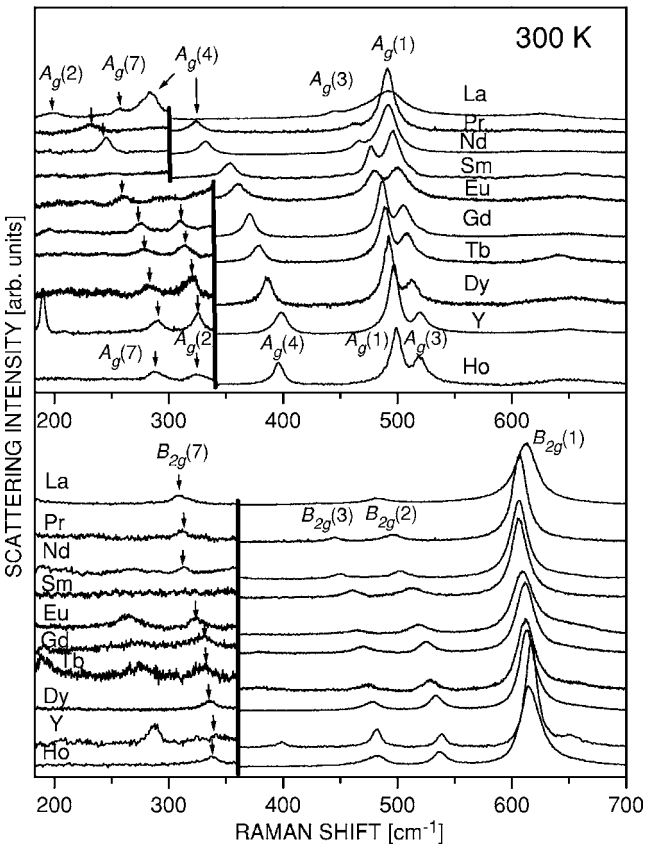

FIG. 1. A_g and B_{2g} Raman spectra of RMnO$_3$ at room temperature. The intensities in the low frequency range are multiplied by factor of 5. The phonon mode notations correspond to those of Refs. 13 and 14. The A_g and B_{2g} spectra are normalized to the integrated intensity of $A_g(1)+A_g(3)$ and $B_{2g}(1)$ lines, respectively. The change of the order of the $A_g(1)-A_g(3)$ and $A_g(2)-A_g(7)$ notations at the two ends of the series is explained in the text.

A. Basic distortions and Raman modes in RMnO$_3$

In the ideal cubic ABO_3 perovskite (space group $Pm\bar{3}m$, Z=1) all atoms are at centrosymmetrical sites with fixed coordinates and there are no Raman-allowed modes. The structure of stoichiometric RMnO$_3$, described at room temperature by the *Pnma* space group (Z=4), can be considered as orthorhombically distorted superstructure of the ideal perovskite with $[100]_o$, $[010]_o$, and $[001]_o$ directions coinciding with the $[101]_c$, $[010]_c$, and $[\bar{1}01]_c$ directions of the parent cubic structure. In the *Pnma* structure the atoms occupy four nonequivalent atomic sites (R,Mn,O1,O2), of them only the Mn site is a center of symmetry. From symmetry considerations only five of the 12 atomic coordinates are fixed [R-1,Mn-3,O1-1], while the remaining seven variable coordinates can be considered as the lattice degrees of freedom producing the above mentioned lattice distortion. These distortions give rise to 24 ($7A_g+5B_{1g}+7B_{2g}+5B_{3g}$) Raman-allowed phonon modes, which in turn can be assigned to their distortions of origin ([010], [101] rotation, JT, or R shift). With decreasing r_R the distortions increase and most of the bond lengths shorten, which reasonably results in a twofold effect: enhanced Raman intensity and hardening of Raman frequencies.

TABLE I. Frequencies (in cm^{-1}) of the experimentally observed A_g and B_{2g} Raman lines of RMnO$_3$ at room temperature. In the last column is given the basic distortion responsible for the mode activation (see Sec. III A).

Mode	Main atomic motions	La	Pr	Nd	Sm	Eu	Gd	Tb	Dy	Ho	Y	Basic distortion
$A_g(1)\rightarrow A_g(3)$	O2 antistretching $\rightarrow$MnO$_6$ bending	490.7	491.2	491.7	496.1	501.0	506.0	509.0	513.4	520.0	520.6	JT,[010]$\rightarrow$[101]
$A_g(3)\rightarrow A_g(1)$	MnO$_6$ bending $\rightarrow$O2 antistretching	444.8	461.8	465.6	476.7	479.0	486.4	488.8	492.1	498.9	496.7	[101]$\rightarrow$JT,[010]
$A_g(4)$	out-of-phase MnO$_6$ x rotations	283.6	323.7	331.8	352.9	360.8	370.5	378.2	386.0	395.9	398.1	[101]
$A_g(2)\rightarrow A_g(7)$	in-phase MnO$_6$ y rotations$\rightarrow$O1(x)	256.8					309.8	314.6	319.5	323.8	325.3	[010]$\rightarrow R$ shift
$A_g(7)\rightarrow A_g(2)$	O1 (x)$\rightarrow$ in-phase MnO$_6$ y rotations	198.1	231.8	245.0	266.1		276.1	280.5		287.8	289.4	R shift $\rightarrow$[010]
$B_{2g}(1)$	in-plane O2 stretching	612.3	606.7	606.2	606.6	609.5	611.7	612.2	613.5	615.0	617.3	JT
$B_{2g}(2)$	in-phase O2 "scissorslike"	482.5	495.7	502.6	513.1	518.4	525.0	528.4	533.6	537.0	539.2	[010]
$B_{2g}(3)$	out-of-phase MnO$_6$ bending	430.0	444.8	449.1	460.9	464.6	468.9	473.7	477.5	481.1	481.5	[101]
$B_{2g}(7)$	O1(z)	309.7	311.5	313.2		323.8	329.2	330.9	335.6		342.0	R shift

At first sight the [010] and [101] rotations can directly be obtained from the O2-Mn-O2 and O1-Mn-O1 angles, which practically have equal values.[10,12] As shown by Abrashev *et al.*,[13] however, even in the case of equal O-Mn-O angles, the [010] and [101] rotation angles will be different. They are related to the deviations (x_i, y_i, z_i, i-atomic index) of *Pnma* atomic coordinates from those in a hypothetical undistorted perovskite structure as

$$\Psi_{[010]} = \arctan(2|x_{O2} - z_{O2}|),$$

$$\Psi_{[101]} = \arctan(2^{5/2}|y_{O2}|) \approx \arctan(2^{3/2}|z_{O1}|).$$

The so-defined atomic deviations can also be used to describe the other two basic distortions, namely, the JT distortion, characterized by the relative difference $D_{JT} = |\Delta d_{Mn-O2}| / \langle d_{Mn-O2} \rangle$ of the two pairs of Mn-O2 distances, and the shift $D_R(x)$ of the R atoms in the x direction from their positions in an undistorted perovskite. In the case of small distortions,

$$D_{JT} = 2|x_{O2} + z_{O2}|,$$

$$D_{R(x)} = 2x_R.$$

The variations of the basic distortions, calculated using the available data for atomic positions in RMnO$_3$,[10,12] are given in Table II.

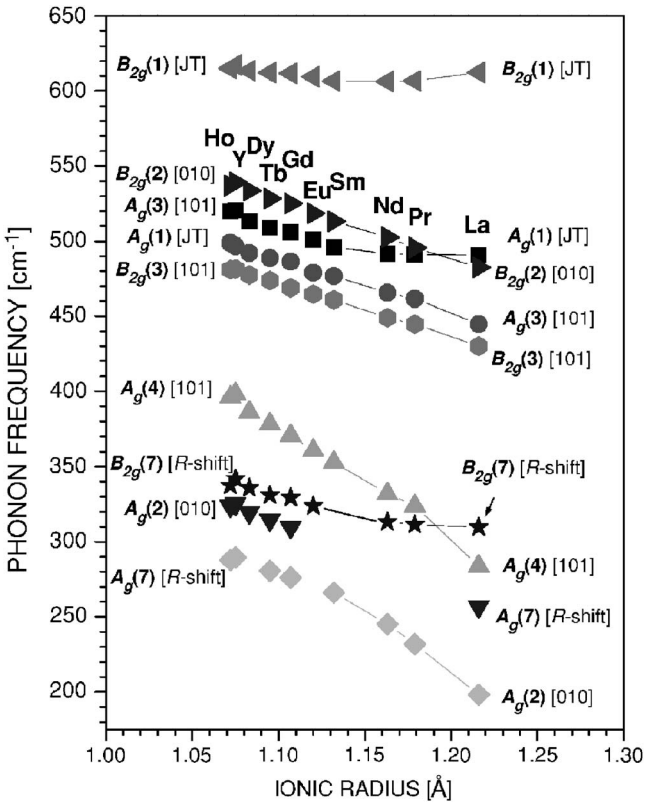

FIG. 2. Variations of phonon mode frequencies with R ionic radius r_R. The notations are explained in Table I and Secs. III A and III B.

B. Pure and mixed stretching (Jahn-Teller) modes

The frequency of a mode involving mainly stretching vibrations of O2 atoms in the xz planes is determined by the Mn-O2 distances. The short and long Mn-O2 bond lengths vary with r_R within 0.5% and 1.1%, respectively,[10,12] and therefore one expects that $\omega_{stretch} \propto d_{Mn-O2}^{3/2}$ will change by no more than 1.5%. As illustrated in Fig. 3, this is exactly the case for the $B_{2g}(1)$ mode at 606–617 cm^{-1}, which has been assigned to the in-phase O2 stretching.[14] The minimum of $B_{2g}(1)$ frequency near R=Nd,Sm reflects the fact that for

TABLE II. Variations with R of the four basic distortions of the *Pnma* structure. The data for $SmMnO_3$ and $GdMnO_3$ have been obtained by the fit of corresponding experimental data for the rest of the $RMnO_3$ compounds (Refs. 10 and 12).

Distortion	Measure	La	Pr	Nd	Sm	Eu	Gd	Tb	Dy	Ho	Y
[010]	$\Psi_{[010]}$ (deg)	9.23	11.43	12.11	13.07	13.35	13.60	13.81	14.00	14.16	14.11
[101]	$\Psi_{[101]}$ (deg)	12.17	13.53	14.08	15.10	15.49	15.86	16.24	16.59	16.90	16.82
JT	$\lvert\Delta d_{\text{Mn-O2}}\rvert/\langle d_{\text{Mn-O2}}\rangle$	0.0647	0.0665	0.0652	0.0612	0.0597	0.0582	0.0574	0.0571	0.0575	0.0573
R shift	$2x_R$	0.097	0.129	0.138	0.151	0.155	0.159	0.166	0.167	0.169	0.168
⟨Mn-O2⟩ (Ref. 10)	Å	2.044	2.063	2.067		2.066			2.065		
⟨Mn-O2⟩ (Ref. 12)	Å	2.043	2.059	2.062				2.063	2.063	2.064	2.052

these R's the averaged Mn-O distance has a maximum.

Based on the same bond-length considerations, one could expect that the Raman line of A_g symmetry at 490–495 cm^{-1}, corresponding to the in-phase antistretching vibrations of O2 in the xz plane,[14] would behave in a similar way and its frequency would remain nearly constant through the whole $RMnO_3$ series. As seen from the top panel of Fig. 3, this is obviously not the case. The data of Figs. 1 and 3 clearly show a classic example for mixing of modes of the same symmetries and close frequencies. For large r_R (R =La,Pr,Nd) the lines at 490–492 and 445–465 cm^{-1} can be considered as pure stretching $[A_g(1)]$ and bending $[A_g(3)]$ modes, respectively. With decreasing r_R the $A_g(3)$ frequency increases and approaches that of $A_g(1)$, resulting in strong mode mixing evidenced by mode repulsion and transfer of intensity. The mixing is most strongly pronounced for R =Sm to Tb where the two modes are of comparable intensities and involve both stretching and bending atomic motions. With further decrease of r_R (R=Dy,Ho,Y) the modes become less mixed but now the higher mode is dominated by MnO_6 bending $[A_g(3)$-type] motions and the lower one is $A_g(1)$ type.

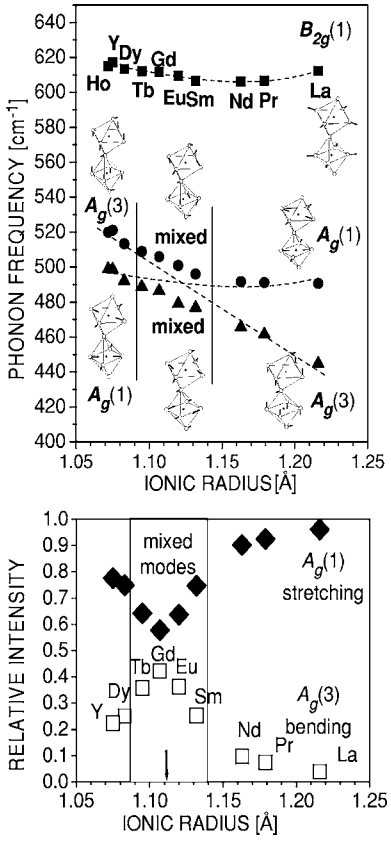

FIG. 3. Top panel: Variations with r_R of the frequencies of $B_{2g}(1)$, $A_g(3)$, and $A_g(1)$ modes. The shown atomic displacements have been determined by lattice dynamical calculations for $R=Y$ and La using a shell model (Ref. 14). The dashed curves show the expected $\omega'(r_R)$ and $\omega''(r_R)$ dependences for pure stretching and bending modes. Bottom panel: Variation with r_R of the relative intensity of $A_g(1)$[mixed $A_g(1)$-like] and $A_g(3)$[mixed $A_g(3)$-like] modes.

Two phonon modes or any other elementary excitations of same symmetries and close frequencies can be considered as coupled quantum oscillators. In a good approximation their frequencies are given by

$$\omega_{1,2} = \frac{\omega' + \omega''}{2} \pm \sqrt{\frac{(\omega' - \omega'')^2}{4} + \frac{V^2}{4}},$$

where ω' and ω'' are the mode frequencies without coupling and V is the coupling constant.[19] It is reasonable to assume that without coupling the $A_g(1)$ and $A_g(3)$ mode frequencies would depend on r_R in the same way as the $B_{2g}(1)$ and $B_{3g}(3)$ modes, respectively, as both modes of the $A_g(1)$-$B_{2g}(1)$ (stretching) and $A_g(3)$-$B_{2g}(3)$ (bending) pairs are activated by the same basic distortion and have similar shape. Therefore, as shown with dashed lines in Fig. 4, the $\omega'(r_R)$ dependence for the uncoupled $A_g(1)$ mode can be approximated by scaling the experimental B_{2g} values, whereas that of uncoupled $A_g(3)$ mode $[\omega''(r_R)]$, such as in the case of $B_{2g}(3)$, can be approximated by a linear dependence. At the crossing point ($r_R \approx 1.125$ Å), $\omega'(1.125)=\omega''(1.125)$, which gives $V=\omega_1(1.125)-\omega_2(1.125)\approx 20$ cm^{-1}.

C. Pure and mixed rotational ("soft") modes

The frequency vs $\Psi_{[101]}$ dependence for the $A_g(4)$ mode involving mainly MnO_6 x rotations, shown in Fig. 4 with full circles, is close to proportionality. Expectedly, this mode exhibits "soft mode" behavior with $\omega(\Psi)\to 0$ for $\Psi\to 0$, the slope of $\omega^{A_g(4)}(\Psi_{[101]})$ being 23.5 cm^{-1}/deg. Calculations of lattice dynamics for the two end compounds $LaMnO_3$ and $YMnO_3$ have shown that the two weak A_g modes at lower

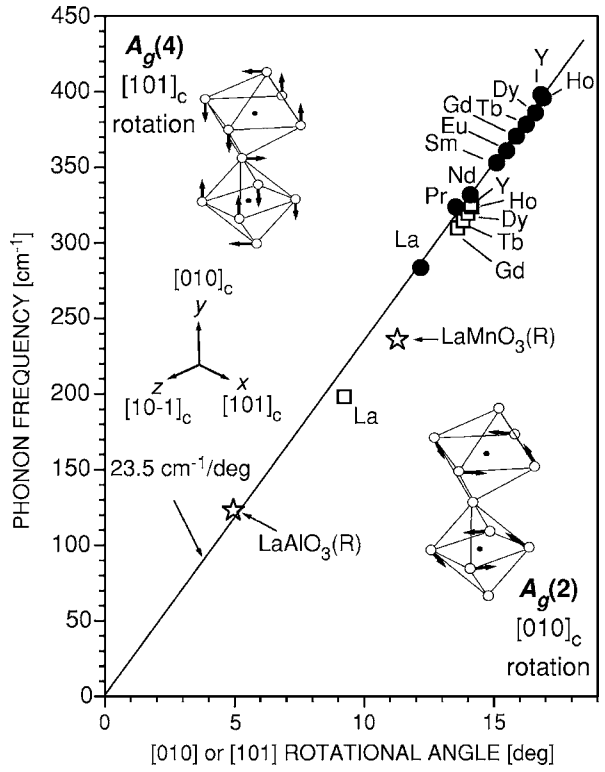

FIG. 4. Variations with the tilt angle $\Psi_{[101]}$ or $\Psi_{[010]}$ of the frequencies of $A_g(4)$ (full circles) and $A_g(2)$ (empty squares) modes, involving mainly MnO_6 rotations (Ref. 14).

frequencies are strongly mixed and involve both in-phase MnO_6 y rotations $[A_g(2)]$ and O1(x) motions $[A_g(7)]$.[14] The higher of these modes is $A_g(7)$-like in $LaMnO_3$, but $A_g(2)$-like in $YMnO_3$. Assuming that the higher mode remains $A_g(2)$-like in other compounds with small r_R ($HoMnO_3$, $DyMnO_3$, $TbMnO_3$, $GdMnO_3$), one finds that the frequency vs $\Psi_{[010]}$ dependence for the partly mixed $A_g(2)$ mode (shown with empty squares) is practically the same as that for the pure $A_g(4)$ mode. Interestingly, the frequencies of [111]-rotational modes of structurally different rhombohedral $LaMnO_3$ and $LaAlO_3$ fit to these dependences, which is an indication for a quite general relationship between the angle of rotation and frequency of the rotational soft modes in perovskitelike compounds, independent on the direction of the rotational axis.

D. *R*-shift modes

The weak $A_g(7)$ and $B_{2g}(7)$ involve mainly O1 motions in the xz plane, activated in the Raman spectrum due to the shift of R^{3+} ions from their positions in an ideal perovskite. It follows from Fig. 2, Table I, and Table II that in the case of pure R-shift mode $[B_{2g}(7)]$, despite strongly increasing R-shift distortion between R=La and Y, the corresponding increase of mode frequency is relatively modest (see Table II). It is plausible to expect similar dependence on r_R for the $A_g(7)$ mode, which explains the above discussed observation that the frequency vs r_R dependence of the mixed $A_g(2)$ $+A_g(7)$ modes is governed mainly by their rotational $[A_g(2)]$ component.

IV. CONCLUSION

The comparative study of polarized Raman spectra of orthorhombic $RMnO_3$ series (R=La,Pr,Nd,Sm,Eu,Gd, Tb,Dy,Ho,Y) shows that the variations of lattice distortions with r_R affect significantly both the phonon frequencies and the shape of some Raman phonon modes. It is an open question whether the strong mixing of phonon modes involving in-plane and out-of-plane oxygen motions plays a role in the change with r_R of magnetic ordering at low temperatures. The established proportionality between the frequency of a rotational mode and the angle of corresponding rotational distortion may be used for material characterization.

ACKNOWLEDGMENTS

This work is supported in part by the State of Texas through the Texas Center for Superconductivity and the National Science and Engineering Research Council of Canada. The work of M.M.G. is supported by the Bulgarian National Research Fund (Contract No. F-1207).

[1] R. M. Kusters, J. Singleton, D. A. Keen, R. McGreevy, and W. Hayes, Physica B **155**, 362 (1989).
[2] R. von Helmolt, J. Wecker, B. Holzapfel, L. Schultz, and K. Samwer, Phys. Rev. Lett. **71**, 2331 (1993).
[3] S. Jin, T. H. Tiefel, M. McCormack, R. A. Fastnacht, R. Ramesh, and L. H. Chen, Science **64**, 413 (1994).
[4] Y. Tokura, A. Urushibara, Y. Moritomo, T. Arima, A. Asamitsu, G. Kido, and N. Furukawa, Science **63**, 3931 (1994).
[5] A. Munoz, M. T. Casáis, J. A. Alonso, M. J. Martinez-Lope, J. L. Martinez, and M. T. Fernández-Díaz, Inorg. Chem. **40**, 1020 (2001).
[6] A. Munoz, J. A. Alonso, M. T. Casais, M. J. Martinez-Lope, J. L. Martínez, and M. T. Fernández-Díaz, J. Phys.: Condens. Matter **14**, 3285 (2002).
[7] T. Kimura, T. Goto, H. Shintani, K. Ishizaka, T. Arima, and Y. Tokura, Nature (London) **426**, 55 (2003).
[8] T. Kimura, S. Ishihara, H. Shintani, T. Arima, K. T. Takahashi, K. Ishizaka, and Y. Tokura, Phys. Rev. B **68**, 060403(R) (2003).
[9] T. Goto, T. Kimura, G. Lawes, A. P. Ramirez, and Y. Tokura, Phys. Rev. Lett. **92**, 257201 (2004).
[10] B. Dabrowski, S. Kolesnik, A. Baszczuk, O. Chmaissem, T. Maxwell, and J. Mais, J. Solid State Chem. **178**, 629 (2005).
[11] B. Lorenz, Y. Q. Wang, Y. Y. Sun, and C. W. Chu, Phys. Rev. B **70**, 212412 (2004).
[12] J. A. Alonso, M. J. Martínez-Lope, M. T. Casais, and M. T. Fernández-Díaz, Inorg. Chem. **39**, 917 (2000).
[13] M. V. Abrashev, J. Bäckström, L. Börjesson, V. N. Popov, R. A. Chakalov, N. Kolev, R. L. Meng, and M. N. Iliev, Phys. Rev. B

65, 184301 (2002).
[14] M. N. Iliev, M. V. Abrashev, H. G. Lee, V. N. Popov, Y. Y. Sun, C. Thomsen, R. L. Meng, and C. W. Chu, Phys. Rev. B **57**, 2872 (1998).
[15] L. Martín-Carrón, A. de Andrés, M. J. Martinez-Lope, M. T. Casais, and J. A. Alonso, Phys. Rev. B **66**, 174303 (2002).
[16] A. M. Balbashov, S. G. Karabashev, Y. A. M. Mukovskii, and S. A. Zverkov, J. Cryst. Growth **167**, 365 (1996).
[17] M. M. Gospodinov *et al.* (unpublished).
[18] M. N. Iliev, B. Lorenz, A. P. Litvinchuk, Y.-Q. Wang, Y. Y. Sun, and C. W. Chu, J. Phys.: Condens. Matter **17**, 3333 (2005).
[19] E. T. Heyen, R. Wegerer, E. Schönherr, and M. Cardona, Phys. Rev. B **44**, 10195 (1991) and references therein.